

# Application of thermal-dissociation laser induced fluorescence (TD-LIF) to measurement of $\text{HNO}_3$ , $\Sigma$ alkyl nitrates, $\Sigma$ peroxy nitrates, and $\text{NO}_2$ fluxes using eddy covariance

D. K. Farmer<sup>1</sup>, P. J. Wooldridge<sup>1</sup>, and R. C. Cohen<sup>1,2</sup>

<sup>1</sup>Department of Chemistry; University of California, Berkeley, Berkeley, CA, 94720, USA

<sup>2</sup>Department of Earth and Planetary Science; University of California, Berkeley, Berkeley, CA, 94720, USA

Received: 22 December 2005 – Published in Atmos. Chem. Phys. Discuss.: 12 April 2006

Revised: 23 June 2006 – Accepted: 28 July 2006 – Published: 22 August 2006

**Abstract.** Nitrogen exchange between the atmosphere and biosphere directly influences atmospheric composition. While much is known about mechanisms of  $\text{NO}$  and  $\text{N}_2\text{O}$  emissions, instrumentation for the study of mechanisms contributing to exchange of other major nitrogen species is quite limited. Here we describe the application of a new technique, thermal dissociation-laser induced fluorescence (TD-LIF), to eddy covariance measurements of the fluxes of  $\text{NO}_2$ , total peroxy acyl and peroxy nitrates, total alkyl and multifunctional alkyl nitrates, and nitric acid. The technique offers the potential for investigating mechanisms of exchange of these species at the canopy scale over timescales from days to years. Examples of flux measurements at a ponderosa pine plantation in the mid-elevation Sierra Nevada Mountains in California are reported and used to evaluate instrument performance.

## 1 Introduction

The exchange of nitrogen between the biosphere and atmosphere affects both oxidative atmospheric chemistry and ecosystem nutrient dynamics, with potential indirect effects on the carbon cycle and climate (Ollinger et al., 2002; Vitousek et al., 1997). Nitrogen enters ecosystems through application of fertilizer, biotic nitrogen fixation of  $\text{N}_2$ , or atmospheric deposition of gaseous or particulate ammonium and oxidized nitrogen, is rapidly cycled in both organic and inorganic forms, and is known to be released from ecosystems to the atmosphere through direct plant emissions of  $\text{NO}$  or  $\text{NO}_2$ , and as a by-product of soil microbial transformations, namely as  $\text{NO}$  or  $\text{N}_2\text{O}$  via nitrification and denitrification. As N is commonly the limiting nutrient for plant growth in forest ecosystems, increased N deposition also increases car-

bon uptake. (Vitousek et al., 1997). This effect has clear implications as the  $\text{CO}_2$  level in the atmosphere continues to rise concurrently with increased anthropogenic N emission and consequent increased N deposition to ecosystems (Sievering et al., 2001). However, because N emissions contribute to ozone formation, increased N deposition associated with those emissions may also be accompanied by increased deposition of ozone. The negative impact of ozone on plant health may offset the positive effects of N deposition on C uptake (Ollinger et al., 2002). As N deposition may lead to increased  $\text{N}_2\text{O}$  emissions and soil respiration, the net C uptake may be further offset (Fenn et al., 1998; Schlesinger and Andrews, 2000). The continued increase in anthropogenic emissions of reactive nitrogen into the atmosphere and nitrogen deposition has led to concerns regarding nitrogen saturation, which may decrease plant health, increase greenhouse gas emissions, and affect water quality (Aber et al., 1998).

Bulk wet and dry nitrate/ammonium deposition has been quantified over numerous ecosystems (e.g. Bobbink et al., 1992; Bytnerowicz and Fenn, 1996; Holland et al., 2005; Shepard et al., 1989 and references therein). More detailed experiments have focused on  $\text{NO}$  and  $\text{N}_2\text{O}$  because of their clear soil sources, the greenhouse warming potential of  $\text{N}_2\text{O}$ , and the availability of commercial detectors (e.g. Davidson and Kinglerlee, 1997; Hanson and Lindberg, 1991; Ludwig et al., 2001; Mosier et al., 2004 and references therein). However, ammonia ( $\text{NH}_3$ ) and the reactive nitrogen oxides ( $\text{NO}_y = \text{NO} + \text{NO}_2 + \text{PAN} + \text{other peroxy nitrates} + \text{alkyl nitrates} + \text{nitric acid} + \text{N}_2\text{O}_5 + \dots$ ) are significant contributors to N dry deposition, and recent research indicates that surface interactions affect atmospheric concentrations and partitioning of these species. For example, extreme changes in the atmospheric reactive nitrogen budget following biomass burning or rain events have been observed (Bertram et al., 2005; Jaegle et al., 2004; Zhang et al., 2002). Few studies have investigated the magnitude and mechanisms of ecosystem-scale exchange of  $\text{NO}_2$ , peroxy nitrates, alkyl nitrates or

Correspondence to: R. C. Cohen  
(rccohen@berkeley.edu)

$\text{HNO}_3$ , likely because of the absence of techniques for measurement of these reactive nitrogen oxide species with both adequate sensitivity and minimal day-to-day maintenance requirements to enable application to ecosystem-scale flux measurements. Eddy covariance (EC) is the most direct method of measuring the exchange of compounds between the atmosphere and earth's surface. (Dabberdt et al., 1993). This technique has stringent requirements for measurements of vertical wind speed and concentration, requiring observations that are fast ( $>1$  Hz), sensitive, portable, and free of interferences (Baldocchi et al., 1988; McMillen, 1988). EC flux measurements of  $\text{NO}_y$ ,  $\text{NO}$ , and  $\text{NO}_2$  fluxes have been reported (e.g. Delany et al., 1986, Horii et al., 2004; Munger et al., 1996; Rummel et al., 2002). Most other studies of N fluxes have used enclosure or indirect estimation techniques, including gradient measurements or resistance modeling (Hanson and Lindberg, 1991; Wesely and Hicks, 2000).

The most extensive measurements are those described by Munger et al. (1996), who observed  $\text{NO}_y$  using eddy covariance at both remote ( $0.003 \text{ ppb m s}^{-1}$  summertime net dry  $\text{NO}_y$  flux, Schefferville, Quebec<sup>1</sup>) and rural ( $0.023 \text{ ppb m s}^{-1}$  summertime,  $0.022 \text{ ppb m s}^{-1}$  wintertime, Harvard Forest) environments. Model results by Munger et al. (1998) indicate that deposition of hydroxyalkyl nitrates,  $\text{HNO}_3$  from heterogeneous reactions of  $\text{N}_2\text{O}_5$  and  $\text{HNO}_3$  from oxidation of  $\text{NO}_2$  by OH contributed comparably to total  $\text{NO}_y$  deposition during summer at Harvard Forest. Horii (2002) found that while the  $\text{NO}_y$  flux at Harvard Forest was explained by  $\text{HNO}_3$  deposition with minor  $\text{NO}_2$  and PAN contributions for unpolluted background flows, up to 50% of the  $\text{NO}_y$  flux in polluted flows was not accounted for by  $\text{NO}_2$ , PAN, and  $\text{HNO}_3$ , and was therefore likely due to alkyl or hydroxyalkyl nitrates and other peroxy or peroxy acyl nitrates.

All published  $\text{HNO}_3$  flux measurements have been either inferential (e.g. Lefer et al., 1999; Tarnay et al., 2001) or indirect (e.g. Huebert et al., 1988; Janson and Granat, 1999; Nemitz et al., 2004; Pryor et al., 2002). Tarnay et al. (2001) used inferential flux measurements at Lake Tahoe, CA, and determined that dry deposition of  $\text{HNO}_3$  is the major source of atmospheric N to the lake.  $\text{HNO}_3$  deposition velocities of  $7.6 \text{ cm s}^{-1}$  were measured at Niwot Ridge using the flux gradient approach (Sievering et al., 2001). Pryor et al. (2002) used both gradient and relaxed eddy accumulation (REA) techniques to measure  $\text{HNO}_3$  fluxes. While downward fluxes were generally observed, Pryor et al. also observed  $\text{HNO}_3$  efflux, potentially due to a chemical flux divergence involving  $\text{HNO}_3$ - $\text{NH}_3$ - $\text{NH}_4\text{NO}_3$  reactions and gas-particle nitrate partitioning, as has also been suggested in several other studies of upward  $\text{HNO}_3$  fluxes (Brost et al., 1988; Huebert et al.,

1988; Neftel et al., 1996; Nemitz et al., 2004; Van Oss et al., 1998).

The sum of alkyl and multifunctional alkyl nitrates ( $\Sigma\text{ANs}$ ), compounds with the formula  $\text{RONO}_2$  where R is any organic functional group, have recently been shown to constitute a significant fraction of atmospheric reactive nitrogen (Cleary et al., 2005; Day et al., 2003; Rosen et al., 2004). While there are few other measurements of alkyl nitrates over forest ecosystems, observations over a boreal forest in Finland using an Aerodyne Aerosol Mass Spectrometer suggested that organic nitrates may be a significant component of biogenic aerosols formed over forests (Allan et al., 2006). Total peroxy acyl and peroxy nitrates ( $\Sigma\text{PNs}$ , compounds with the formula  $\text{RO}_2\text{NO}_2$  (peroxy nitrates) or  $\text{RC(O)O}_2\text{NO}_2$  (peroxy acyl nitrates)) and  $\Sigma\text{ANs}$  may include hydroxyl substituted species that are highly soluble in water, and are thus likely to strongly interact with the biosphere. Leaf-scale studies demonstrated that plants can directly uptake peroxyacetyl nitrate (PAN), demonstrating a mechanism for dry deposition of PAN (Sparks et al., 2003; Teklemariam and Sparks, 2004). Laboratory measurements have demonstrated uptake of PAN by an alfalfa canopy occurs with a deposition velocity of  $0.75 \text{ cm s}^{-1}$  (Hill, 1971). However, observational evidence for strong daytime PAN deposition on an ecosystem scale is equivocal. For example, Doskey et al. (2004) used the modified Bowen ratio technique to measure daytime PAN deposition velocities over a grassland site; while upward PAN fluxes were observed during sunny afternoons, possibly due to chemistry associated with emission of precursor compounds, net PAN fluxes averaged over three months were downward with an average deposition velocity of  $0.13 \pm 0.13 \text{ cm s}^{-1}$ . Nighttime velocity measurements using  $^{222}\text{Rn}$  and PAN concentrations showed significant, though variable, deposition (Schrimpf et al., 1996), as had been indicated by previous studies (Shepson et al., 1992). Recent eddy covariance flux measurements of PAN showed rapid deposition, particularly to wet surfaces (Turnipseed et al., 2006). The potential for exchange of organic nitrates between ecosystems and the atmosphere is particularly important to consider more carefully following research suggesting that organic nitrates play an important role in ecosystem nutrient cycling (Bragazza and Limpens, 2004; Neff et al., 2002; Perakis and Hedin, 2002).

While NO is generally observed to be emitted from soils (e.g. Gasche and Papen, 2002; Jaegle et al., 2004; Rummel et al., 2002), both emission and deposition of  $\text{NO}_2$  have been observed using eddy covariance over grasslands and fields (Delany et al., 1986; Wesely et al., 1982). At Harvard Forest, Horii observed downward NO fluxes and upward  $\text{NO}_2$  fluxes. (Horii, 2002).  $\text{NO}_x$  fluxes are complicated by rapid within-canopy radical reactions that occur on a chemical timescale faster than that of the physical exchange, i.e. flux divergence. (Vila-Guerau de Arellano et al., 1993). Following emission from soils, NO reacts with  $\text{O}_3$  to produce  $\text{NO}_2$ , thus decreasing the observed NO upward flux, and potentially causing a

<sup>1</sup>Note that  $1 \text{ ppb m s}^{-1} = 147 \mu\text{mol m}^{-2}\text{hr}^{-1} = 0.57 \mu\text{g (N)m}^{-2}\text{s}^{-1}$ .

net upward  $\text{NO}_2$  flux. Thus the potential for within-canopy oxidation, measurement height above the canopy, and other factors affecting canopy and atmospheric  $\text{NO}_x$  levels to affect the observed  $\text{NO}$ ,  $\text{NO}_2$  and  $\text{O}_3$  fluxes. This flux divergence has been observed in an Amazonian rain forest, where  $\text{NO}$  emissions from the soil were observed near the surface, but were not significant above the canopy (Rummel et al., 2002).  $\text{NO}_x$  fluxes are further complicated by direct leaf exchange that may lead to the presence of a compensation point. A compensation point is the atmospheric mixing ratio above which a compound is deposited and below which the compound is emitted. Compensation points for  $\text{NO}_2$  of 0.53–1.60 ppb were reported for different plant species by Sparks et al. (2001).

Here we present the application of thermal dissociation – laser induced fluorescence (TD-LIF), a new technique for measuring mixing ratios of  $\text{NO}_2$ , total peroxy nitrates ( $\Sigma\text{PNs}$ ), total alkyl and multifunctional alkyl nitrates ( $\Sigma\text{ANs}$ ), and  $\text{HNO}_3$  (Day et al., 2002), to eddy covariance measurements. We evaluate the performance of the instrument based on field experiments at a mid-elevation ponderosa pine plantation in the Sierra Nevada Mountains and describe some of the observations.

## 2 Site

Field measurements were made in summer and fall of 2003 (June–November) and from the summer 2004 through spring of 2005 (May 2004–June 2005) above a ponderosa pine plantation planted in 1990 in the mid-elevation (1315 m) Sierra Nevada Mountains. The trees were about 9 m tall in 2004. The plantation is owned by Sierra Pacific Industries and is near the University of California at Berkeley's Blodgett Forest Research Station (UC-BFRS,  $38^\circ 53' 42.9'' \text{N}$ ,  $120^\circ 3757.9'' \text{W}$ ) (see Goldstein et al., 2000 for complete description). The inlets and sonic anemometer were located  $\sim 12$  m above the ground on a walk-up tower, and  $\sim 3$  m above the top of the canopy; the TD-LIF detector is located in a temperature-controlled shed located just north-east of the tower. The site is characterized by a Mediterranean climate with a cold, wet season (October–April) and a warm, dry season (May–September). In the summer, daytime winds are predominantly southwest ( $210$ – $240^\circ$ ), upslope from the Sacramento Valley. Nighttime winds are from the northeast ( $30^\circ$ ), downslope from the Sierra Nevada. A diesel generator provides power to the site, and is located  $\sim 130$  m to the north of the tower.

## 3 Instrumentation

Measurements of  $\text{NO}_2$ ,  $\Sigma\text{PNs}$ ,  $\Sigma\text{ANs}$ , and  $\text{HNO}_3$  were made with the Berkeley thermal dissociation-laser induced fluorescence instrument (TD-LIF) (Day et al., 2002; Thornton et al., 2000). Briefly, air is pulled simultaneously through a

single inlet manifold into four channels, each of which consists of an inlet, heated section of quartz tube (“oven”) and LIF  $\text{NO}_2$  detector. Each class of compounds ( $\Sigma\text{PNs}$ ,  $\Sigma\text{ANs}$ ,  $\text{HNO}_3$ ) thermally dissociates to  $\text{NO}_2$  and an accompanying radical ( $\text{RO}_2$ ,  $\text{RO}$ ,  $\text{OH}$ ) at a characteristic temperature. The ovens are separately thermostatted at  $550^\circ\text{C}$ ,  $330^\circ\text{C}$ ,  $180^\circ\text{C}$ , and ambient temperature (Day et al., 2002). At  $180^\circ\text{C}$ ,  $\Sigma\text{PNs}$  dissociate to  $\text{NO}_2$  and the signal in that channel is the sum of  $\text{NO}_2 + \Sigma\text{PNs}$ . The  $330^\circ\text{C}$  channel adds  $\Sigma\text{ANs}$ , and the  $550^\circ\text{C}$  channel  $\text{HNO}_3$  to the total. Mixing ratios of each class ( $\Sigma\text{PNs}$ ,  $\Sigma\text{ANs}$ , and  $\text{HNO}_3$ ) are the difference in  $\text{NO}_2$  observed in channels set at adjacent temperatures; for example, the difference in  $\text{NO}_2$  detected in the  $330^\circ\text{C}$  channel and  $180^\circ\text{C}$  channel is the  $\Sigma\text{ANs}$  mixing ratio. No filters were placed in front of the inlet, thus both gaseous and particulate  $\text{NO}_y$  compounds are measured. Bertram and Cohen (2003) demonstrated evaporation and detection of semi-volatile  $\text{NH}_4\text{NO}_3$  aerosol to  $\text{NO}_2$  in the  $550^\circ\text{C}$  channel with  $>0.8$ , and likely unit, efficiency, and that non-volatile aerosols (e.g.  $\text{NaNO}_3$ ) are not detected; semi-volatile organic nitrate aerosols are expected to evaporate and be detected in the  $330^\circ\text{C}$  oven. Thus our reported  $\text{HNO}_3$  is the sum of gas and semi-volatile aerosol N and our  $\Sigma\text{ANs}$  are the sum of gas and semi-volatile aerosol  $\Sigma\text{ANs}$ .

Our technique for LIF detection of  $\text{NO}_2$  is described in detail in Thornton et al. (2000) and Day et al. (2002). Briefly, a custom-built, tunable dye laser is pumped at 8 kHz by a compact, diode-pumped, Q-switched frequency-doubled  $\text{Nd}^{3+}$ -YAG laser (Spectra Physics, average power of 3 W at 532 nm, 30 ns pulse length). The dye laser (pyromethene-597 in isopropanol) emits a 25 ns wide (FWHM) pulse at 585 nm (linewidth  $0.06 \text{ cm}^{-1}$ ), and is tuned to a specific, narrow rovibronic feature of  $\text{NO}_2$ . The dye laser tuning is alternated between this strong  $\text{NO}_2$  resonance and a weaker continuum absorption to test for interferences, assess background scatter, and maintain a frequency-lock on the spectral feature of interest. The instrument chop cycle is maintained at 20 s on-resonance, followed by 5 s off-resonance. The laser light is focused through each of four multipass (White) cells in series. We collect the red-shifted ( $>700 \text{ nm}$ ) fluorescence photons with cooled GaAs photomultiplier tubes (Hamamatsu H7421-50) using time-gated single-photon counting. The fluorescence signal, collected at 5 Hz, is directly proportional to the  $\text{NO}_2$  mixing ratio. The cell pressure is reduced to  $\sim 3$  Torr using a roots blower (Eaton M-62 supercharger) backed by an oil-sealed rotary vane pump. These pumps maintain a flow of  $\sim 1500 \text{ sccm}$  through each of the four cells (total flow of 6000 sccm).

Comparisons between the TD-LIF and independent measurement techniques demonstrate the ability of TD-LIF to adequately measure  $\text{NO}_{y,i}$ . Thornton et al. (2003) showed that the daily average agreement between  $\text{NO}_2$  mixing ratios observed by photolysis to  $\text{NO}$  followed by chemiluminescence (PCL) and LIF was better than 5% in Nashville, TN during the 1999 Southern Oxidant Study and again outside

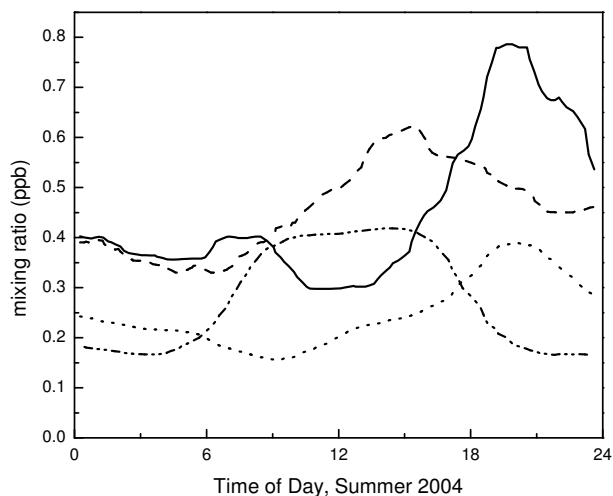


**Fig. 1.** Average mixing ratios (ppb) by time of day from August–September 2004 of  $\text{NO}_2$  (—), total peroxy nitrates (---), total alkyl nitrates (···), and  $\text{HNO}_3$  (-·-·-).

of Houston during TEXAQS-2000. Comparisons between the  $\Sigma\text{PNs}$  measured by TD-LIF and  $\Sigma\text{PAN}_i$  ( $=\text{PAN} + \text{PPN} + \text{PiBN} + \text{MPAN} + \text{APAN}$ ) measured by GC-ECD during the TexAQS-2000 study in LaPorte, TX showed agreement within 6% (Rosen, 2004).  $\text{NO}_y$  measured by chemiluminescence was on average within 1% during the daytime with  $\Sigma\text{NO}_{y_i}$  ( $=\text{NO}_2$  (TD-LIF) +  $\Sigma\text{PNs}$  (TD-LIF) +  $\Sigma\text{ANs}$  (TD-LIF) +  $\text{HNO}_3$  (TD-LIF) +  $\text{HONO}$  (DOAS) +  $\text{NO}_3$  (DOAS) +  $\text{NO}$  (CL) +  $\text{NO}_3^-$  (aerosol) (PILS)) during the TexAQS-2000 campaign (Rosen, 2004).

We define the sensitivity of this  $\text{NO}_2$  measurement technique as that mixing ratio for which the signal to noise for a given averaging time is equal to 2. Thus the sensitivity depends on the calibration constant and background signal rate, which vary with laser power and cell alignment. The  $\text{NO}_2$  signal is calculated as

$$S_{\text{NO}_2} = S_{\text{total}} - B \quad (1)$$

where  $S_{\text{NO}_2}$  is the  $\text{NO}_2$  signal,  $S_{\text{total}}$  is the total LIF counts measured during the experiment and  $B$  is the background, or mean of LIF counts measured in zero air. Because the background signal is obtained from an average over several minutes, random error in  $B$  is negligible compared to errors in  $S_{\text{total}}$ , which is obtained over 0.2 s. The noise in the  $\text{NO}_2$  signal is given by Poisson statistics as  $\sqrt{S_{\text{total}}}$ , or  $\sqrt{S_{\text{NO}_2} + B}$ . Over the course of the campaign described here, the sensitivity ranged from 24 pptv in 0.2 s to 64 pptv in 0.2 s due to degradation of laser performance. Maintenance was performed every 4–7 days to optimize the sensitivity. As described in Day et al. (2002), because each class of compounds is calculated as the difference in signals observed in adjacent cells, the uncertainty for each compound is a func-

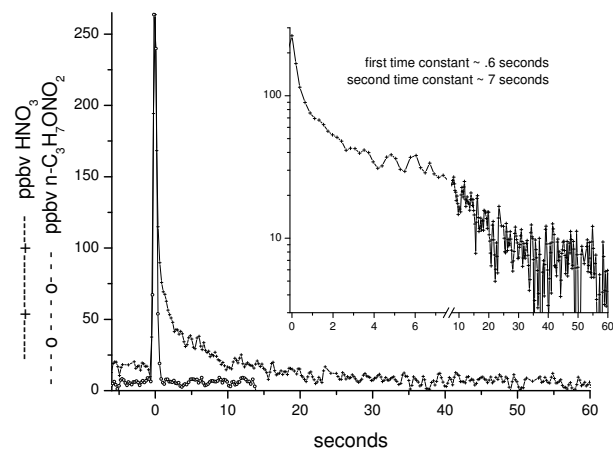


**Fig. 2.** Response to  $\text{HNO}_3$  and n-propyl nitrate spike tests in the laboratory. The inset illustrates the recovery after the  $\text{HNO}_3$  spike.

tion of both instrument sensitivity and mixing ratios measured in adjacent channels:

$$(S_A - S_B) \pm (\Delta_A^2 + \Delta_B^2)^{1/2} \quad (2)$$

where  $S_A$  and  $S_B$  are the signals from adjacent channels, and  $\Delta_A$  and  $\Delta_B$  are their associated uncertainties, as calculated above for  $\text{NO}_2$ . The instrument's sensitivity to the difference in adjacent channels, e.g. for  $\Sigma\text{PNs}$ , is calculated considering  $S/N=2 = (S_A - S_B) / (\Delta_A^2 + \Delta_B^2)^{1/2}$ . For typical background counts and calibration constants, the sensitivity for  $\Sigma\text{PNs}$  above a 1 ppb background of  $\text{NO}_2$  is 66 ppt in 0.2 s.

As  $\text{HNO}_3$  adsorbs strongly even to Teflon surfaces at ambient temperatures and humidities (e.g. Neuman et al., 1999), a fast response inlet was designed to minimize  $\text{HNO}_3$  loss before air enters the two hot ovens ( $550^\circ\text{C}$ ,  $330^\circ\text{C}$ ). This inlet, similar to that described by Day et al. (2002), was also designed to minimize dust and prevent insects from entering the sampling lines. The fore region of the inlet, which allows the addition of calibration and zero flows, is made of extruded PFA (perfluoroalkoxy) Teflon tubing and injection-molded compression PFA fittings (Swagelok). Hot processed (extruded or molded) parts appear to be significantly better than those machined from PFA bar stock, presumably because hot processing leaves a smoother, more closed surface. To minimize the losses at high relative humidity, most of the inlet plumbing is thermostatted at  $60^\circ\text{C}$ , a temperature high enough to prevent  $\text{HNO}_3$  wall loss, but low enough to prevent unintended dissociation of  $\Sigma\text{PNs}$  during the transit time. The inlet manifold is designed to minimize flow distortion, to ensure that flows are identical, and to maintain identical inlet residence times for all four channels. The manifold consists of two identical 1"-diameter short tubes, which draw air into the fore region in which air is sub-sampled and split into one of two adjacent ovens. The two outer tubes are

vertically displaced by 0.05 m, and are placed 0.30 m behind the sonic anemometer in the prevailing daytime wind direction. The heater sections are 0.25–0.3 m long and 0.4 mm I. D. quartz; the quartz continues for another 0.6–0.8 m to allow the gas to cool before reaching the junction to the PFA tubing ( $\sim 18$  m) that carries the  $\text{NO}_2$  product to the detection cells. A pressure-reducing orifice is incorporated into this junction, decreasing the pressure and shortening the transit time from the inlet.

We characterized the time responses for  $\text{HNO}_3$  and n-propyl nitrate by spiking concentrated samples in front of the inlet and monitoring the resulting signal (Fig. 2). The primary time constants for the rise and fall for both species are  $\leq 0.6$  s, though a low-amplitude secondary decay with a time constant of  $\sim 7$  s was observed for  $\text{HNO}_3$ , but not n-propyl nitrate. As these measurements were spikes to laboratory air (containing 30–40 ppbv  $\text{NO}_y$ , relative humidity  $\sim 30\%$ ), the  $\text{HNO}_3$  and n-propyl nitrate released remained in the laboratory, causing non-zero background mixing ratios after the spikes.

A sonic anemometer (Campbell Scientific CSAT3 3-D Sonic Anemometer) located on the tower, pointing into the daytime wind direction, at the same height and 0.3 m in front of the TD-LIF inlet, measures wind speed in three dimensions (sample rate of 5 Hz), allowing for wind direction and virtual temperature to be calculated.

#### 4 Data processing

Fluorescence collected by the PMTs was converted to mixing ratio using a standard calibration procedure (Day et al., 2002). Each step in this procedure was reinvestigated in detail to check that it did not produce unintended contributions to the flux. Briefly, data were normalized to the running mean of the entrance laser power for each cell, as observed separately for the on and off-resonance measurements. The line-locking protocol varies the dye-laser frequency about the center of the  $\text{NO}_2$  absorption peak. The maximum absorbance is observed to coincide with the maximum fluorescence and we correct the fluorescence signal by comparing the on-resonance absorbance to the local maximum in absorbance measured through the  $\text{NO}_2$  reference cell.

Background counts due to chamber scatter, PMT dark noise, and any residual  $\text{NO}_2$  in the system, were measured by overflowing the inlet with zero air (Sabio, Model 1001 Portable Air Source) for 170 s at 30 min intervals. Background counts for the ambient channel were typically  $< 5$  counts per second (cps), or  $\sim 40$  ppt  $\text{NO}_2$ . The instrument was calibrated every 2 h with an  $\text{NO}_2$  standard (NIST-traceable 4.77 ppm  $\text{NO}_2(\pm 5\%)$  with 0.2 ppm NO in  $\text{N}_2$ , Praxair CA) diluted to 1–10 ppb in zero air. The calibration standard was compared to other NIST-traceable  $\text{NO}_2$  standards in our lab at least once a year, and was found to be stable in  $\text{NO}_2$  mixing ratio. The calibration mixture was

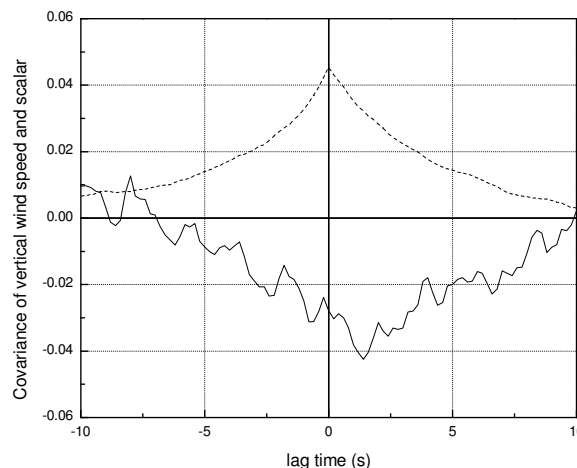


**Fig. 3.** The lag correlation diagram demonstrates that the covariance ( $\text{ppb m s}^{-1}$ ) for the vertical wind speed and  $550^\circ\text{C}$  ( $\Sigma\text{NO}_{y_i}$ ) TD-LIF channel (solid line) maximizes at a lagtime of 1.4 s for this half-hour in the late morning of 17 September 2004. The sensible heat covariance ( $^\circ\text{C m s}^{-1}$ , divided by 10, dashed line) maximizes at 0 s.

transported in separate lines from the pure zero air to prevent residual  $\text{NO}_2$  from affecting background measurements, and was introduced as an overflow at the inlet so that it passes through the ovens and sampling lines before being detected. The mixing ratio data were corrected ( $< 5\%$ ) for quenching by water (Thornton et al., 2000).

Spikes in  $\text{NO}_x$  caused by the diesel generator are occasionally observed during periods of light, variable winds, most often at night. Data influenced by spikes were identified and removed by first flagging data points in which  $\text{NO}_2$  or  $\text{NO}_y$  varied by more than 5 standard deviations from the mean for a given half hour, and then by removing any remaining spikes by hand.

Data from the sonic anemometer were processed by rotating the wind vectors for each half hour to ensure that the vertical wind measurements were taken normal to the shear plane (Baldocchi et al., 1988; McMillen, 1988). Data from the sonic anemometer and the LIF system are acquired at the same rate (5 Hz) and on the same computer using programs that run independently. Nonetheless, the data points do not necessarily coincide exactly in time, and may be shifted by  $< 0.2$  s. To correct for this problem, we linearly interpolate the LIF data onto the sonic anemometer time stamp prior to flux analysis.

The finite length of tubing between the inlet at the top of the tower and the LIF detection sensor on the ground causes a time lag in measurements taken by the sonic and TD-LIF systems. This time lag is the sum of time taken for a given parcel of air to move past the sonic anemometer and into the inlet,

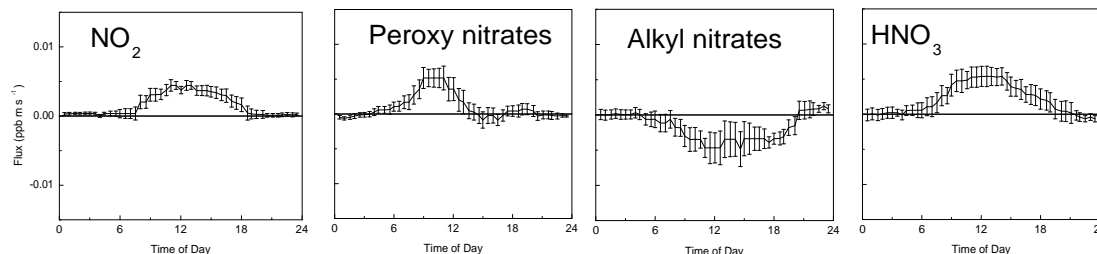


**Fig. 4.** Average fluxes (running mean with standard error,  $\text{ppb m s}^{-1}$ ) of  $\text{NO}_2$ ,  $\Sigma\text{PNs}$ ,  $\Sigma\text{ANs}$  and  $\text{HNO}_3$  from the summer (June–August) 2004.

which is a function of wind speed and distance between the inlet and anemometer, plus the time taken for the air to move from the inlet into the LIF chamber, which is a function of tube length and pumping speed. The pumping speed varied daily with air density, which depends on atmospheric pressure and temperature. However, the effect of these variations on lag time was minor ( $<0.5$  s), and did not affect observed fluxes. While the length of sample tubing was roughly the same for each sample line, slight differences in the pinhole size for each sampling line and the arrangement of vacuum tubing from the Roots blower to the LIF chambers caused the pressure in each chamber to be slightly different (between 2.7 and 3.1 Torr), and thus the lagtimes to be different for each channel. This lagtime is accounted for in the EC analysis by shifting the LIF detector data by an appropriate number of data points (lagtime) to align with the sonic data for each of the four channels. The lagtime is determined from plots of the covariance between the sonic and LIF detector at varying lagtimes; a peak in these lagged covariance plots occurs at the lagtime required for the sample air to move through the sample tubing (Fig. 3). As expected, no lagtime is observed between the vertical wind speed and temperature as the vertical wind speed and virtual temperature are derived from measurements taken on the same instrument. The maximum covariance observed in a lagged covariance plot for mixing ratio and vertical wind speed is the EC flux. The typical lagtime for a given pump and tubing configuration was determined for each channel, and applied to the dataset; the pump and tubing configuration changed several times throughout the campaign (summer 2003 to summer 2005) due to pump failures. For example, for the summer of 2004, we applied lags of 2.2 s for the  $550^\circ\text{C}$  channel, 2.0 s for the 330 and  $180^\circ\text{C}$  channels, and 2.6 s for the ambient  $\text{NO}_2$  channel.

## 5 Mixing ratios

$\text{NO}_y$  mixing ratios at UC-BFRS are between 0.5–3 ppb and exhibit a diurnal trend of increasing mixing ratio with the upslope wind during the day, maximizing in the late evening, and decreasing when the downslope flows return cleaner

air until late morning (Day, 2003; Dillon et al., 2002). Unlike other rural sites,  $\text{NO}_y$  maxima in the summer are higher than in the winter (Day, 2003). We attribute this to stronger transport from urban source areas during summer. During the study period, typical  $\text{NO}_x$  mixing ratios range from 0.2 to 1.0 ppb;  $\Sigma\text{PNs}$  from 0.1 to 1.0 ppb;  $\Sigma\text{ANs}$  from 0.05 to 0.5 ppb, and  $\text{HNO}_3$  0.01 ppb to 1.0 ppb. The statistics of  $\text{NO}_{y_i}$  mixing ratios are described in detail in Murphy et al. (2006). Ozone mixing ratios ranged from 35 to 70 ppb. Mid-day ozone fluxes are about  $0.306\text{--}0.340 \text{ ppb m s}^{-1}$  ( $45\text{--}50 \mu\text{mol m}^{-2} \text{ h}^{-1}$ ) in the summer, and  $0.102 \text{ ppb m s}^{-1}$  ( $15 \mu\text{mol m}^{-2} \text{ h}^{-1}$ ) in the winter (Kurpius and Goldstein, 2003). Figure 1 shows the median summer mixing ratios of  $\text{NO}_2$ ,  $\Sigma\text{PNs}$ ,  $\Sigma\text{ANs}$  and  $\text{HNO}_3$  versus time of day.

## 6 Eddy covariance fluxes

The EC flux for a given species,  $F_c$ , is calculated as the covariance between the vertical wind speed and species mixing ratio,

$$F_c = \frac{1}{n} \sum_{i=1}^n (w_i - \bar{w}) \cdot (c_i - \bar{c}) \quad (3)$$

where  $n$  is the number of points used for the calculation,  $w_i$  and  $c_i$  are instantaneous measurements of vertical wind speed and mixing ratio, and  $\bar{w}$  and  $\bar{c}$  are the mean vertical wind speed and mixing ratio respectively. A positive flux indicates upwards movement of mass from the surface to the atmosphere. Measurements are typically taken for  $\sim 30$  min at 5 Hz, which is both long and fast enough to capture all flux-carrying eddies. Fluxes measured by the EC method are valid only if the assumptions behind Taylor's "frozen flow" hypothesis are met, namely that eddies move past the tower unchanged and in stationary flow (Stull, 1988).

The eddy covariance technique requires that the calculated fluxes do not vary within time-scales of analysis, the stationarity requirement. We tested for stationarity by comparing the 30-min flux  $\langle w'c' \rangle_{30 \text{ min}}$  to the mean of fluxes calculated from the six consecutive 5-min samples within the half hour,

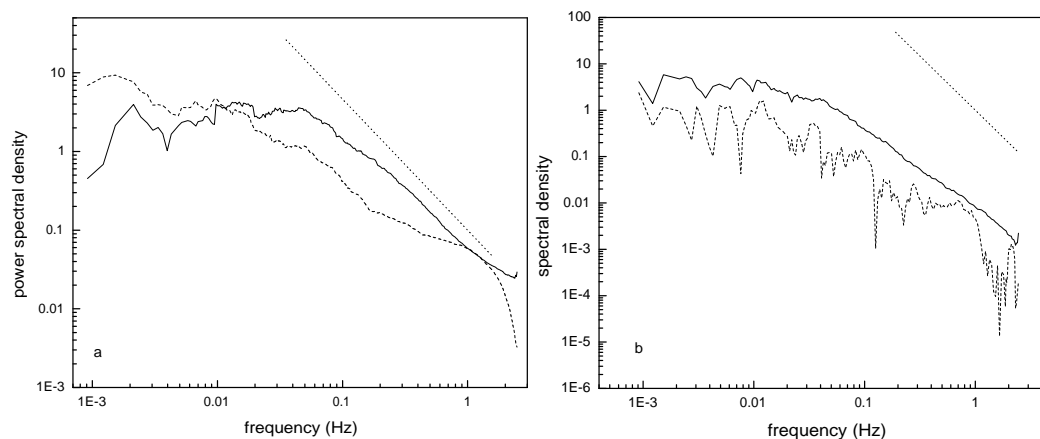


**Fig. 5.** (a) Power spectrum of vertical wind speed (solid line) and NO<sub>2</sub> (dashed line) observed during a single half hour in the afternoon of 17 September 2004; a line with a  $-5/3$  slope indicates the presence of an inertial subrange. (b) Cospectra of vertical wind speed and temperature (solid line) and vertical wind speed and NO<sub>2</sub> (dashed line) for the same half-hour as (a). A line with a  $-7/3$  slope indicates the presence of an inertial subrange. Note that the power spectra are binned into 500 evenly spaced intervals along the logarithmic frequency axis; cospectra are similarly binned into 200 intervals.

$\overline{\langle w'c' \rangle}_{5 \text{ min}}$ . Data for which the ratio of sub-set flux mean to half-hour mean was not within  $\pm 30\%$  (Foken and Wichura, 1996),

$$0.7 < \frac{\overline{\langle w'c' \rangle}_{5 \text{ min}}}{\overline{\langle w'c' \rangle}_{30 \text{ min}}} < 1.3, \quad (4)$$

were assumed to be non-stationary. More than 95% of the previously filtered NO<sub>y,i</sub> data from the winter season (January–March 2005) were stationary. The sensible heat fluxes are not filtered for spikes due to the nearby generator prior to analysis, and only met the stationarity criterion for 67% during winter 2005. For September 2004, more than 93% of NO<sub>y,i</sub> data not influenced by the generator were stationary, while 66% of the sensible heat data were stationary. Most of the non-stationary sensible heat fluxes were at times when spikes from the generator were observed.

Nighttime EC CO<sub>2</sub> fluxes are typically filtered to exclude data observed in low turbulence regimes, as determined by a threshold friction velocity ( $u_*$ ) ranging from 0.0 to 0.6 m s<sup>-1</sup> (Massman and Lee, 2002). These filters are often applied when CO<sub>2</sub> fluxes correlate with friction velocity at low  $u_*$ , which should not occur because CO<sub>2</sub> fluxes are assumed to be driven by biological controls, and thus uncorrelated to turbulence (Massman and Lee, 2002). However, as the controlling mechanisms of NO<sub>2</sub>, ΣPNs, ΣANs, and HNO<sub>3</sub> fluxes are poorly understood, there is no clear evidence that the fluxes are biologically determined. Thus we have not removed nighttime data that has passed the stationarity test, although nighttime  $u_*$  at Blodgett Forest ranged from 0.01 to 0.5 m s<sup>-1</sup> during September 2004. Future work will analyze the long-term NO<sub>y,i</sub> flux dataset from Blodgett to determine whether a  $u_*$  threshold should be applied.

As fluxes are calculated from the deviations from the mean for a given scalar, a time-varying mean mixing ratio causes spurious fluxes. We used a 10-min running mean to calculate the perturbations from the mean for scalar mixing ratio and vertical wind speed,  $c'$  and  $w'$ . The turbulent flux for a given half hour is the average of the product of these two values,  $\langle c'w' \rangle$  (McMillen, 1988). Sensitivity tests determined that the 10-min running mean was long enough to capture trends caused by movement of pollutant plumes and chemical changes; inspection of cospectra (see below) shows that the low frequency eddies that are removed using 10-min means were not important to the total flux. Similar to mixing ratio measurements, fluxes were determined for each of the four channels, and the difference between adjacent channels gives the flux for each class. This is theoretically identical to calculating fluxes by taking the difference between appropriately lagged channels, and calculating the flux for each class of species. The theoretical conclusion was borne out in practice, as identical fluxes were calculated either way i.e.  $F(\text{NO}_2(T2) - \text{NO}_2(T1)) = F(\text{NO}_2(T2)) - F(\text{NO}_2(T1))$  where NO<sub>2(T)</sub> refers to the total NO<sub>2</sub> observed at a particular oven temperature. No density corrections are required for the eddy flux measurements as the TD-LIF measures the mixing ratio of a species in the atmosphere rather than the absolute concentration (Webb et al., 1980). All mixing ratio and flux analysis programs were written specifically for this instrument.

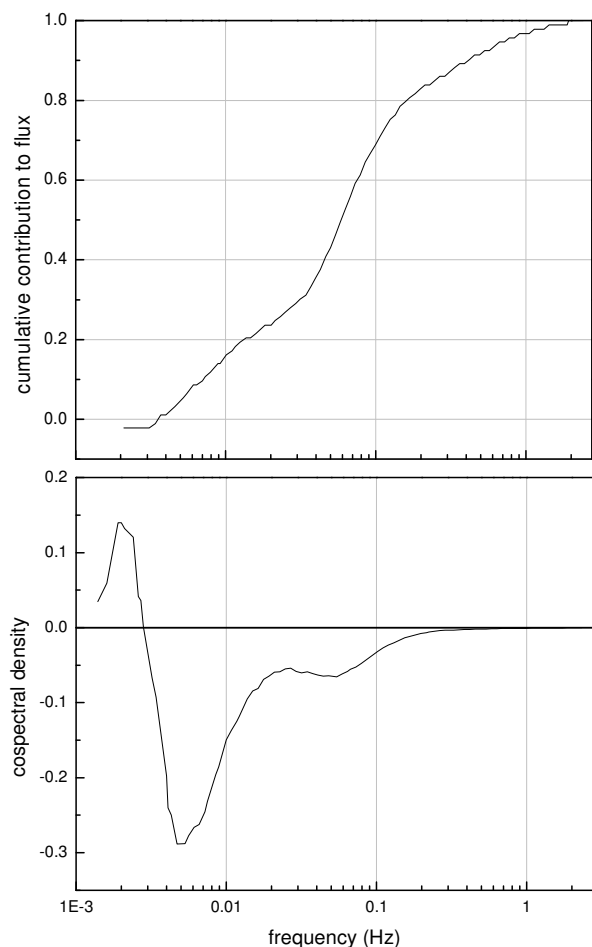


**Fig. 6.** Normalized cumulative contribution to the flux (a) and averaged semilogarithmic cospectrum (b) and from all daytime data of  $\Sigma$ ANs for 1 August–10 August 2004. The cospectrum is binned into 100 evenly spaced intervals along the frequency axis.

## 7 Spectral analysis

EC measurements are known to be challenging because of the wide dynamic range in frequency required of the sensors. We test the TD-LIF fluxes using a variety of spectral analyses that demonstrate the experimental capabilities. Figures 1 and 3 show mean mixing ratios and fluxes for summer 2004 (June–August). Eddy covariance fluxes are potentially subject to underestimation by systematic errors due to 1) time lags between the sonic anemometer and mixing ratio measurements and 2) damping of high frequency fluctuations. Time lags between mixing ratio and wind measurements are accounted for as described above. Damping of high frequency fluctuations may be caused by sensor separation, smoothing of flows in the sensor lines, and limited sensor response time.

The magnitude of underestimation of fluxes due to the separation distance between the sonic anemometer and the chemical inlet depends on the mean wind speed. The flux underestimation can be calculated for lateral (perpendicular to wind direction) and longitudinal (parallel to wind direction) separation using a spectral transfer function (Moore, 1986):

$$T_s(f) = e^{-9.9 f^{1.5}} \quad (5)$$

where  $f = \frac{n \cdot s}{U}$  is the normalized frequency for which the function is being calculated,  $n$  is frequency (Hz),  $s$  is the separation distance (m), and  $U$  is the mean wind speed ( $\text{m s}^{-1}$ ). To evaluate the loss of total flux due to sensor separation, we compared observed cospectra that were corrected by this transfer function to the uncorrected cospectra. The lateral separation between the TD-LIF inlets and sonic anemometer is  $<0.05$  m, and results in a negligible effect on the flux; a 0.05 m separation and mean wind speeds of 0.5, 1.5, 5, and  $10 \text{ m s}^{-1}$  correspond to underestimation by 1.82, 0.22, 0.03, and 0.01%. The longitudinal separation is 0.3 m. A 0.30 m separation distance and mean wind speeds of 0.5, 1, 2, and  $10 \text{ m s}^{-1}$  cause underestimation by  $>99\%$ , 83.3%, 6.2%, and  $<0.2\%$ . For median daytime windspeeds of  $3 \text{ m s}^{-1}$  this effect is an error of less than 1%. At night when wind speeds are typically  $1 \text{ m s}^{-1}$ , this effect can cause significant attenuation of the flux. However, Moore (1986) points out that this transfer function does not consider wind direction and likely overestimates the loss. We ignore flow distortion due to the inlet and sonic anemometer as the anemometer is faced into the prevailing daytime wind direction. The tilt angle is the angle required to rotate the sonic anemometer vectors about the horizontal axis to give a mean vertical wind speed of zero, and provides an indication of flow distortion (Goulden et al., 1996). The tilt angle for 30-min intervals is always less than  $10^\circ$  from zero, and indicates only minor flow distortion from either tower shadowing or the inlet set up (McMillen, 1988). The  $3.69^\circ$  ( $0.03 = \text{standard deviation}$  from the mean,  $N=3023$ ) tilt angle for winds in the  $200\text{--}360^\circ$  (SSW–N) direction (1 July 2004 to 30 November 2004), which account for over 75% of daytime winds, has little variability demonstrating negligible flow distortion for daytime winds over the fetch. The variability in tilt angle is greater in the  $100\text{--}150^\circ$  wind directions ( $-1.3^\circ$ ,  $\sigma=0.06$ ,  $N=2821$ ), demonstrating that passing through the tower (NE–SE winds) affects turbulence. Nighttime fluxes will be more significantly impacted, as only  $\sim 35\%$  of the winds originate in the  $200\text{--}360^\circ$  direction. As the variance in tilt angle in the prevailing wind direction is relatively small, the inlet design likely does not cause significant flow distortion.

When fluids pass through long sample tubes, the high frequency fluctuations are dampened by smearing due to the different speeds traveled by fluctuations being carried at different frequencies, or spectral attenuation (Lenschow and Raupach, 1991). We calculate the half-power fluctuation damping frequency of the sample tubing ( $1/8$ "i.d.) according to



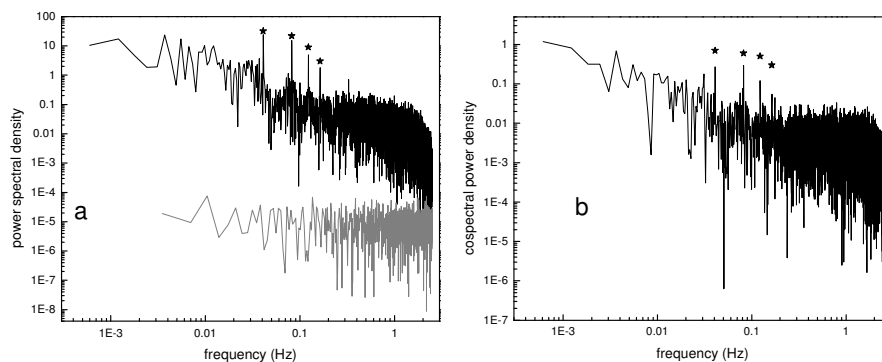


**Fig. 7.** Unsmoothed power spectra (a) of  $\Sigma\text{NO}_{\text{y}}$  (black) and instrument noise (grey) for this channel, and cospectrum (b) of  $\Sigma\text{NO}_{\text{y}}$  and vertical wind speed for a single half hour; stars are at 0.04, 0.08, 0.12, and 0.16 Hz marking the frequency and harmonics of the etalon chop cycle.

Lenschow and Raupach (1991); this is the frequency at which half the spectral power is lost due to attenuation. The half-power damping frequency is  $\sim 6$  Hz for our system. Damping at this frequency will result in minimal attenuation of  $\text{NO}_{\text{y}}$  fluxes as cospectra show that most of the  $\text{NO}_{\text{y}}$  flux is carried by turbulence occurring on significantly slower timescales. A spectral correction may be applied to data to account for this dampening effect on observable fluctuations. One commonly used correction technique is to apply a transfer function to the cospectra to determine the fractional error of the measured flux, and to account for signal loss (Massman, 1991; Moore, 1986). Application of Massman's transfer function to typical cospectra from our dataset demonstrates that under most circumstances  $<2\%$  of the flux is lost due to spectral attenuation. In rare circumstances when the calculated lagtimes indicate a slower flow through the tubing, losses as high as 7% are calculated.

Power spectra of both the observed vertical wind speed and LIF mixing ratio data are level at the low frequencies (0.02 Hz), showing that the measurement interval of 30 min is long enough to capture the low frequency eddies that carry flux (Fig. 5a). The spectrum for only one channel is presented because all four channels have very similar spectra, as expected for identical inlet configurations and detection techniques. The power spectra have  $(\text{frequency})^{-5/3}$  behavior for frequencies between 0.02 and 0.8 Hz, indicative of the inertial subrange and demonstrating that the TD-LIF sensitivity is adequate to measure mixing ratio perturbations due to turbulence (Anderson et al., 1986). At frequencies greater than  $\sim 1$  Hz the mixing ratio power spectra become noise limited as indicated by the rapid fall off in spectral density.

Cospectra of vertical wind speed and temperature and vertical wind speed and mixing ratio both show the same slopes, and both deviate from the expected  $(\text{frequency})^{-7/3}$  slope in the same way (Fig. 5b). This behavior is characteristic of the inertial subrange between 0.01–0.8 Hz. Again, all four chan-

nels produce similar logarithmic cospectra. The slopes for both TD-LIF and sonic anemometer cospectra are more shallow than the  $-7/3$  slope expected from Komolgorov theory, which can not be due to spectral attenuation, as this should not occur in the sensible heat cospectra. The  $-7/3$  slope is predicted from dimensional analysis, and deviations are not unprecedented. In long-term studies of turbulence spectra over two mixed hardwood forests, Su et al. (2004) observed turbulence spectra with shallower slopes in the inertial subrange than the expected. Blanken et al. (1998) similarly observed cospectral slopes in the inertial subrange less than theoretically expected for fluxes of sensible heat, water and  $\text{CO}_2$  both above and below a boreal aspen forest. The shallow cospectra slopes observed in this study suggest that the cascade of energy transfer from larger to smaller eddies in the inertial subrange occurs with a power law smaller than the  $-7/3$  suggested by dimensional analysis. The cospectra on a semi-logarithmic scale (Fig. 6) further demonstrate that the main contributions to flux are from eddies in the 0.01 to 0.5 Hz frequency range (corresponding to 6–300 m horizontally for a  $3 \text{ m s}^{-1}$  wind) (Anderson et al., 1986; Kaimal et al., 1972). This frequency range is similar to the 0.005 to 0.5 Hz range observed for  $\text{NO}_y$  by Munger et al. (1996), and confirms that the TD-LIF time response is adequate. The structure observed within the TD-LIF cospectra can be removed by averaging data in larger frequency bins, but is potentially indicative of complex process controlling  $\text{NO}_{\text{y}}$  fluxes, and was thus preserved in Fig. 5. The data also confirm that measurements with characteristic time constants significantly shorter than the maximum 0.6 s TD-LIF time constant would have been of limited additional benefit. Loss of flux signal from the instrument time constant can be approximated as:

$$\frac{F_m}{F_t} = \frac{1}{(1 + 2\pi f_m \tau)} \quad (6)$$

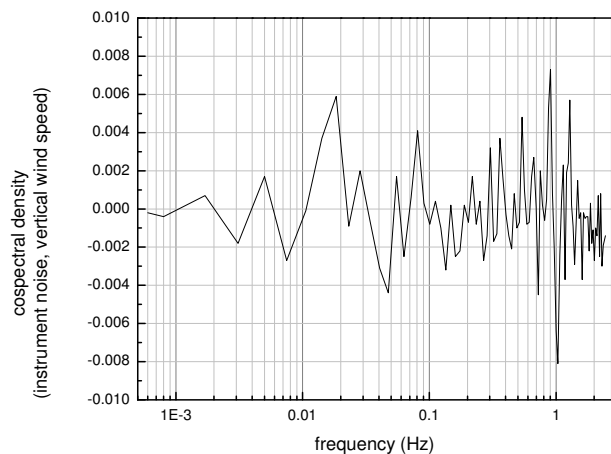


**Fig. 8.** Cospectrum of instrument noise (zero air measurements) and vertical wind speed, demonstrating the lack of covariance and thus minimal impact of noise on observed fluxes. This cospectrum is binned into 94 evenly spaced intervals along the logarithmic frequency axis.

where  $F_m$  is the observed flux,  $F_t$  is the true flux,  $f_m$  is the frequency at which the frequency-multiplied cospectrum maximizes, and  $\tau$  is the first-order response time of the sensor (Horst, 1997). For  $f_m$  of 0.01 Hz and  $\tau$  of 0.6 s, the underestimation is 3.6% for the  $\text{HNO}_3$  flux. As these are conservative estimates of  $f_m$  and  $\tau$ , we do not correct for this underestimation in the fluxes presented in Fig. 4.

To test for interferences and prevent drift of the laser frequency, the TD-LIF measurement algorithm alternates the laser frequency on and off the  $\text{NO}_2$  resonance in a 25 s cycle. However, imperfections in the instrument calibration at the on and off resonance frequencies will introduce fluctuations at 25 s (0.04 Hz), which could potentially covary with fluctuations in the vertical wind speed, causing spurious fluxes. The power spectra (e.g. Fig. 7a) show a clear, narrow peak at 0.04 Hz, as well as the harmonics of this signal at 0.08, 0.12, and 0.16 Hz (marked with stars). The cospectra of mixing ratio and vertical wind speed (Fig. 7b) still have peaks at 0.04 Hz and its harmonics, but they are dampened because the chop cycle is independent of fluctuations in the vertical wind speed. The potential effect of the chop cycle on fluxes was quantified by integrating the area under the semi-log cospectrum in the frequency regions affected by the chop cycle and determined to be negligible (<1%).

The LIF-vertical wind speed cospectra are less coherent than the sensible heat cospectra derived solely from the sonic anemometer (Fig. 5b). The high-frequency ( $\geq 1$  Hz) noise is possibly due to higher instrument noise in the LIF detector than the sonic anemometer. The variations at lower frequencies for the mixing ratio cospectra are more likely due to chemical reactions and the fact that production and deposition of certain species is inhomogeneous within the fetch,

causing varying mixing ratios in the horizontal plane, thus affecting observed fluxes and cospectra (Delany et al., 1986). Future studies will include a more thorough analysis of these variations.

Instrument noise may correlate with vertical wind speed resulting in a spurious flux, contributing to uncertainty in the observed scalar flux. We determine this uncertainty both theoretically and experimentally. The contribution to flux variance due to instrument noise,  $\sigma_{\text{inst}}^2(F; T)$ , can be written as

$$\sigma_{\text{inst}}^2(F; T) = \frac{\sigma_w^2 \sigma_n^2 \Delta t}{T} \quad (7)$$

where  $\sigma_w^2$  and  $\sigma_n^2$  are the variance in vertical wind speed ( $\text{m}^2 \text{s}^{-2}$ ) and instrument noise ( $\text{ppb}^2$ ) respectively,  $\Delta t$  is the sampling interval (0.2 s for 5 Hz measurements), and  $T$  is the averaging time (s) (Lenschow and Kristensen, 1985; Ritter et al., 1990). As the instrument noise is dominated by shot noise, the variance in instrument noise can be calculated for each half hour sampling interval as the square root of the total number of photon counts, converted to mixing ratio units by the appropriate calibration constant. The photon counts vary with scalar mixing ratio and laser alignment within each White cell. The calculated contribution to error in the measured fluxes from instrument counting noise is calculated as the square root of  $\sigma_{\text{inst}}^2$ . For example, for typical noon-time  $\sigma_w^2$  of  $0.7 \text{ m}^2 \text{ s}^{-2}$  and instrument shot noise of 0.01 ppb, the  $\sigma_{\text{inst}}^2(F; T)$  is  $7.8 \times 10^{-9} \text{ ppb}^2 \text{ m}^2 \text{ s}^{-2}$ , causing an uncertainty of  $8.8 \times 10^{-5} \text{ ppb m s}^{-1}$  ( $0.013 \mu\text{mol m}^{-2} \text{ hr}^{-1}$ ) for a half hour of 5 Hz data. On a typical day the average uncertainty in the flux ranged from  $1.4 \times 10^{-6} \text{ ppb m s}^{-1}$  for the  $550^\circ\text{C}$  channel to  $2.9 \times 10^{-5} \text{ ppb m s}^{-1}$  for  $\text{NO}_2$ . These calculated contributions to error in the measured fluxes are orders of magnitude less than the measurements. The contribution to flux uncertainty for  $\Sigma\text{PNs}$ ,  $\Sigma\text{ANs}$  and  $\text{HNO}_3$  is calculated by propagation of the contributions from adjacent channels. For example, the error for fluxes centered around noon of 10 September 2004, a typical summer day, are calculated to be  $7.0 \times 10^{-5}$ ,  $3.7 \times 10^{-5}$  and  $1.4 \times 10^{-5} \text{ ppb m s}^{-1}$  for  $\Sigma\text{PNs}$ ,  $\Sigma\text{ANs}$ , and  $\text{HNO}_3$ , respectively.

Zero-air measurements provide experimental validation that TD-LIF fluxes are not dominated by instrument noise. Zero air was flowed into the inlet continuously for  $\sim 30$  min in the morning of 10 September 2004, and the observed LIF signals in each channel were combined with sonic anemometer data to calculate a zero-air flux. Because TD-LIF measurements rely on differences between the channels there might be additional contributions to the error budget of a measurement associated with imperfect subtraction that are not captured by these zero air fluxes. However we have found no evidence for such effects. The zero air fluxes are single-point measurements of instrument noise to flux. Because the variance is the integral of a power spectrum, comparison of the power spectra of a half-hour of zero air (Fig. 7a, grey) to a half hour of  $\Sigma\text{NO}_{\text{yi}}$  (Fig. 7a, black)

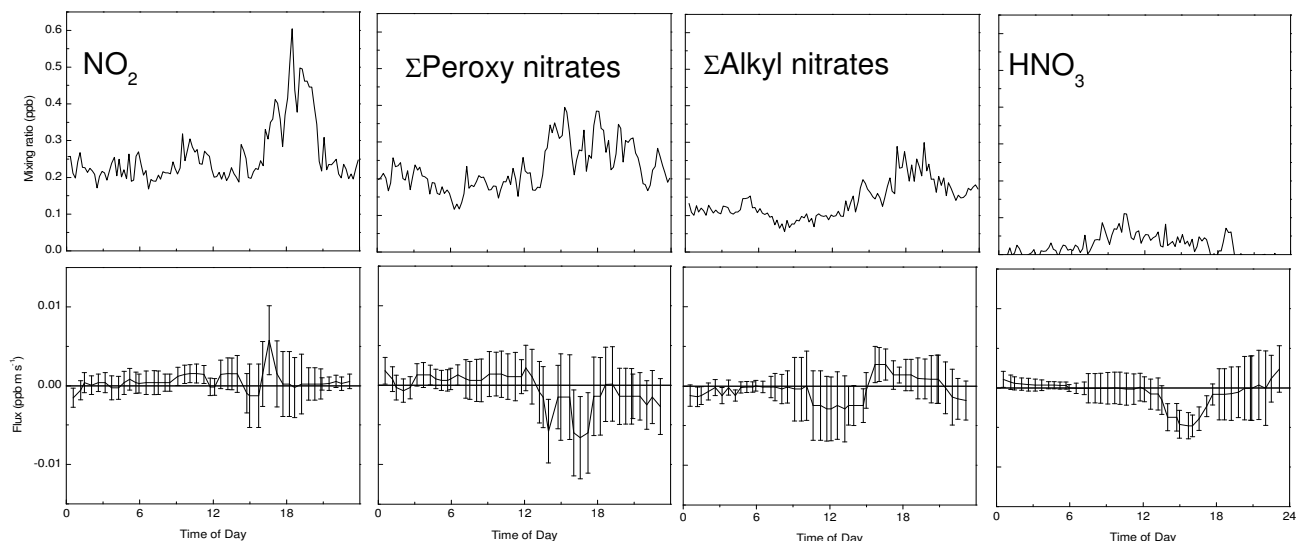


**Fig. 9.** (a–d). Average mixing ratios (ppb, upper panels) and fluxes (running mean with standard error,  $\text{ppb m s}^{-1}$ , lower panels) of  $\text{HNO}_3$ ,  $\Sigma$ alkyl nitrates,  $\Sigma$ peroxy nitrates, and  $\text{NO}_2$  for winter (1 January–31 March 2005).

demonstrates that the variance in measured  $\Sigma\text{NO}_{\text{yi}}$  is minimally affected by variance in instrument noise. The cospectrum of instrument noise (Fig. 8) is completely flat with a maximum amplitude of  $0.008 \text{ ppb m s}^{-1}$  independent of frequency, compared to typical mixing ratio fluxes (Fig. 5b) which exhibit an inertial sub-range. We calculated fluxes from the half-hour of measurements of zero-air with 30 min intervals of vertical wind speed data following protocols identical to our EC flux calculations for atmospheric data. The maximum and minimum noise flux for 10 September 2004 were  $3.8 \times 10^{-4}$  and  $1.3 \times 10^{-6} \text{ ppb m s}^{-1}$  for the  $550^\circ\text{C}$  channel, and  $4.6 \times 10^{-3}$  and  $5.9 \times 10^{-6} \text{ ppb m s}^{-1}$  for the ambient  $\text{NO}_2$  channel. For the differences between channels we observe maximum zero air fluxes of  $6.3 \times 10^{-5}$ ,  $7.5 \times 10^{-3}$ , and  $1.2 \times 10^{-3} \text{ ppb m s}^{-1}$  and minimum fluxes of  $6.3 \times 10^{-5}$ ,  $5.8 \times 10^{-6}$ , and  $6.9 \times 10^{-7} \text{ ppb m s}^{-1}$  for  $\Sigma\text{PNs}$ ,  $\Sigma\text{ANs}$ , and  $\text{HNO}_3$ . For reasons we cannot fully explain, these measurements are an order of magnitude larger than the error calculated using Eq. (7), though they are still small compared to the measured fluxes. As an example, Table 1 compares observed fluxes with theoretical and experimental estimates of noise for the half-hour at noon on 10 September 2004.

These zero fluxes can be used to estimate a minimum observable flux using the TD-LIF method of subtracting adjacent channels. As fluxes for  $\Sigma\text{PNs}$ ,  $\Sigma\text{ANs}$ , and  $\text{HNO}_3$  are calculated as a difference in fluxes of adjacent channels ( $F_{\text{diff}}$ ), we can consider the flux measurement sensitivity due to instrument noise similarly to the above calculations of the random component of uncertainties and sensitivities in mixing ratio data:

$$F_{\text{diff}} = F_A - F_B \pm \Delta_{F_a}^2 + \Delta_{F_b}^2)^{1/2} \quad (8)$$

For 10 September 2004, with a  $S/N = 2 = F_A - F_B / (\Delta_{F_a}^2 + \Delta_{F_b}^2)^{1/2}$ , where  $\Delta_{F_a}$  and  $\Delta_{F_b} = 1.6 \times 10^{-5}$  and  $1.1 \times 10^{-4} \text{ ppb m s}^{-1}$  for the  $\text{HNO}_3$  channel, we calculate that  $|F_A - F_B| \geq 2.2 \times 10^{-4} \text{ ppb m s}^{-1}$  ( $0.032 \mu\text{mol m}^{-2} \text{ hr}^{-1}$ ) will have  $S/N > 2$ . Similarly, the minimum observable flux is  $2.2 \times 10^{-4}$  and  $6.0 \times 10^{-4} \text{ ppb m s}^{-1}$  for  $\Sigma\text{ANs}$  and  $\Sigma\text{PNs}$  respectively. While it is difficult to generalize this estimate of a detection limit because it depends both on the instrument sensitivity and on the variance of the vertical winds, we do find that daytime fluxes are almost always a factor of 10–100 larger than the uncertainty estimated from the zero air measurement, and that nighttime fluxes when  $u_* < 0.1 \text{ m s}^{-1}$  may sometimes have signal to noise less than 2.

## 8 Patterns in the fluxes

The fluxes and mixing ratios observed at Blodgett Forest represent a large and complex dataset that will be discussed in detail in future manuscripts.

The mean winter fluxes (Fig. 9) demonstrate the potential of the TD-LIF method when coupled to EC. Wintertime  $\Sigma\text{NO}_{\text{yi}}$  fluxes are dominated by midday deposition of  $\Sigma$ peroxy nitrates,  $\Sigma$ alkyl nitrates and  $\text{HNO}_3$ , while  $\text{NO}_2$  exhibits a variable, if slightly upward, flux. The net downward flux of  $\Sigma\text{ANs}$  and  $\Sigma\text{PNs}$  flux is a sign of the potentially important role of deposition of these organic nitrogen species to the forest ecosystem during winter. Upward  $\text{NO}_2$  fluxes may be due to a combination of several processes. As the  $\text{NO}_2$  mixing ratios are low, a compensation point may cause plants

**Table 1.** Errors in eddy covariance fluxes from TD-LIF instrument noise from half-hour centered around noon, 10 September 2004.

Channel	Observed Flux (ppb m s <sup>-1</sup> )	Theoretical noise (ppb m s <sup>-1</sup> ) (relative error)	Zero air flux (ppb m s <sup>-1</sup> ) (relative error)
550°C ( $\Sigma\text{NO}_{y_i}$ )	0.0184	$3.44 \times 10^{-6}$ (0.02%)	$1.50 \times 10^{-5}$ (0.08%)
330°C ( $\Sigma\text{ANs} + \Sigma\text{PNs} + \text{NO}_2$ )	.0173	$1.40 \times 10^{-5}$ (0.08%)	$3.38 \times 10^{-4}$ (1.95%)
180°C ( $\text{NO}_2 + \Sigma\text{PNs}$ )	0.0467	$3.37 \times 10^{-5}$ (0.07%)	$-1.9 \times 10^{-3}$ (4.1%)
Ambient ( $\text{NO}_2$ )	0.0196	$6.17 \times 10^{-5}$ (0.31%)	$1.8 \times 10^{-3}$ (9.2%)

within the ecosystem to release  $\text{NO}_2$ , as observed on the leaf scale for tropical plants (Sparks et al., 2001). As the ground was covered by snow during the winter, a direct release of  $\text{NO}_2$  as a result of snow photochemistry could also cause emission (Domine and Shepson, 2002). A third mechanism potentially responsible for the upward  $\text{NO}_2$  fluxes is emission of NO, either from plants (Wildt et al., 1997) or snow (Domine and Shepson, 2002), followed by reaction with  $\text{O}_3$  in the canopy, resulting in a net observed upward flux. Fluxes of all species are significantly smaller at nighttime than daytime, likely due to the low turbulence ( $u_* < 0.17 \text{ m s}^{-1}$ ) and significant attenuation. Further, as the nighttime wind direction is in the opposite direction from the sonic anemometer, air may have to pass through the tower before reaching the inlet and anemometer, causing perturbations to the turbulence and removing the stickier  $\text{HNO}_3$  and hydroxyl-alkyl nitrates.

During the winter, mixing ratios of  $\Sigma\text{NO}_y$  are lower than in the summer (Figs. 1, 9). Regional winds in the winter are weaker, preventing the Sacramento air plume from reaching Blodgett Forest much of the time. The variability in mixing ratio likely contributes to the variability in observed deposition. By normalizing the flux by mixing ratio, we can obtain the deposition velocity,  $V_{\text{dep}}$ :

$$V_{\text{dep}} = \frac{-F}{C} \quad (9)$$

where  $F$  is the flux and  $C$  is the mixing ratio. The  $V_{\text{dep}}$  is typically thought of as the result of a molecule passing through a series of resistances between the atmosphere and ecosystem,

$$V_{\text{dep}} = \frac{1}{R_a + R_b + R_c} \quad (10)$$

where  $R_a$  is the aerodynamic resistance,  $R_b$  is the laminar boundary-layer resistance and  $R_c$  is the canopy resistance. The observed  $V_{\text{dep}}$  derived from flux and mixing ratio measurements can be compared to the theoretical maximum  $V_{\text{dep}}$ , or  $V_{\text{max}}$ , which assumes that the gas is always absorbed by the ecosystem surfaces (i.e.  $R_c = 0$ ). To calculate a  $V_{\text{max}}$ , we estimated  $R_a$  and  $R_b$  by the Dry Deposition Inferential Method from observed windspeeds and

$u_*$  (Hicks et al., 1987). The average summer  $V_{\text{max}}$  was 0.042 to  $0.047 \text{ m s}^{-1}$  in the daytime, and 0.0 to  $0.008 \text{ m s}^{-1}$  at night. The average winter  $V_{\text{max}}$  showed significantly more variability, ranging from 0.015 to  $0.044 \text{ m s}^{-1}$  in the daytime, and between 0 and  $0.015 \text{ m s}^{-1}$  at night. The median  $V_{\text{dep}}$  for  $\text{HNO}_3$  during winter afternoons between 11:00–13:00 PST was  $0.025 \text{ m s}^{-1}$ , and 80% of the data fall between  $V_{\text{dep}}$  of  $-0.012$  and  $0.082 \text{ m s}^{-1}$ . For  $\Sigma\text{ANs}$  the median  $V_{\text{dep}}$  was  $0.021 \text{ m s}^{-1}$ , and 80% fell in the range 0.013 to  $0.18 \text{ m s}^{-1}$ , while for  $\Sigma\text{PNs}$  the median  $V_{\text{dep}}$  was  $0.0084 \text{ m s}^{-1}$ , and the 80% range is  $-0.0057$  to  $0.063 \text{ m s}^{-1}$ . The observed  $V_{\text{dep}}$  for all species measured by TD-LIF were significantly less, suggesting that either the resistance model overestimates the resistances, or that canopy resistances were significant, which is likely the case for all species other than  $\text{HNO}_3$ . Further, observed  $\text{HNO}_3$  and  $\Sigma\text{ANs}$  fluxes may be affected by semi-volatile components. The contribution of ammonium nitrate aerosol ( $\text{NH}_4\text{NO}_3$ ) is expected to be minor at Blodgett Forest as there are no local  $\text{NH}_3$  sources, and any  $\text{NH}_3$  or  $\text{NH}_4\text{NO}_3$  originating from the agricultural region of the Central Valley are expected to have deposited by the time the air mass has reached Blodgett Forest. Observations at Whitaker Forest in the western Sierra Nevada, closer to agricultural sources than Blodgett Forest, measured  $\text{NH}_4\text{NO}_3$  mixing ratios less than 0.15 ppb during the summer Bytnerowicz and Riechers, 1995). Particulate  $\text{NH}_4\text{NO}_3$  is expected to deposit to surfaces, though with a slower  $V_{\text{dep}}$  than gas-phase  $\text{HNO}_3$  due to an increased aerodynamic resistance; the resulting effect on observed TD-LIF  $\text{HNO}_3$  fluxes would be diminished deposition rates, and thus a smaller  $V_{\text{dep}}$ . To our knowledge, there are no specific studies of particulate alkyl nitrates in forest regions, though aerosol measurements by Allan et al. (2006) over a boreal forest suggested that organic nitrates may have a particulate component that would, if present, reduce the observed  $V_{\text{dep}}$ .

The net exchange of  $\Sigma\text{NO}_{y_i}$  over a given period can be derived by integrating the total flux over the time period of interest. Unfortunately, generator failures and instrumental problems at Blodgett Forest occurred throughout the winter,

**Table 2.** Summary of errors affecting TD-LIF eddy covariance fluxes, with conservative estimates of relative contribution to flux.

Source of Error	Bias	Relative error (1 m/s mean wind speed)		Relative error (5 m/s mean wind speed)		Error analysis reference
Sensor separation, lateral	Underestimate	< 0.43%		< 0.03%		Moore, 1986
Sensor separation, longitudinal	Underestimate	< 20.2		< 0.25%		Moore, 1986
Spectral attenuation	Underestimate	< 7% (typically, <2%)				Lenschow & Raupach, 1991
Instrument time response	Underestimate	< 3.6%				Horst, 1997
Chop cycle	None	< 1%				this work
Instrument noise	None	< 2% <sup>a</sup>				Lenschow & Kristensen, 1985, Ritter et al. 1990
Instrument noise	None	< 15% <sup>b</sup>				this work

a=For lowest instrument sensitivities kept in this dataset b=For typical results by channel, see Table 1

and resulted in a patchy dataset that included only a third of the winter days (1 January 2005–31 March 2005). To determine the net exchange, we integrated the average winter diurnal cycle of  $\Sigma\text{NO}_{\text{y}}$  fluxes, and multiplied by 90 days. Assuming that the median winter cycle adequately represents the winter exchange, Blodgett Forest experiences  $0.102 \text{ kg N ha}^{-1}$  dry  $\Sigma\text{NO}_{\text{y}}$  deposition in the winter. No previous measurements of dry deposition have been made at UC-BFRS, though estimates of summer deposition fluxes to Ponderosa pines at Whitaker's Forest, which is south of UC-BFRS, from a foliage rinsing technique estimated annual dry deposition ( $\text{NO}_3^- + \text{NH}_4^+$ , gas + particle) of  $1.0$ – $1.5 \text{ kg N ha}^{-1}$  (Bytnerowicz and Riechers, 1995). Other studies suggest the Sierra Nevada receives an average of  $1.7 \text{ kg N ha}^{-1} \text{ yr}^{-1}$  wet ( $\text{NO}_3^- + \text{NH}_4^+$ ) deposition. (Bytnerowicz and Fenn, 1996). Measurements at Lake Tahoe, which is higher in elevation and further east than Blodgett, indicate summertime dry deposition ( $\text{HNO}_{3(\text{g})} + \text{NH}_{3(\text{g})} + \text{NH}_4\text{NO}_{3(\text{p})}$ ) ranging from  $1.2$ – $8.6 \text{ kg N ha}^{-1} \text{ yr}^{-1}$  for the summer and fall, versus wet deposition ( $\text{NO}_3^- + \text{NH}_4^+$ ), which ranges from  $1.7$  to  $2.9 \text{ kg N ha}^{-1} \text{ yr}^{-1}$  (Tarnay et al., 2001). The TD-LIF-derived estimate of dry deposition of  $\text{NO}_{\text{y}}$  species during the winter at Blodgett Forest is lower than total N deposition measurements elsewhere in the Sierra Nevada, likely because of higher  $\text{HNO}_3$  mixing ratios in the summer and high  $\text{HNO}_3$  mixing ratios closer to direct  $\text{NO}_x$  sources in California's Central Valley or from tourism within the Lake Tahoe basin. While the TD-LIF derived dry deposition estimate does not include contributions of reduced N, these compounds are expected to be minor at Blodgett Forest, and should not contribute strongly to a deposition flux.

Mean summer fluxes (Fig. 4) are characterized by upward fluxes in  $\text{NO}_2$ ,  $\Sigma\text{PNs}$ , and  $\text{HNO}_3$ , and downward fluxes of  $\Sigma\text{ANs}$ . The net upward  $\text{NO}_2$ ,  $\Sigma\text{PNs}$  and  $\text{HNO}_3$  fluxes suggest that within canopy chemistry competes with deposition for these reactive nitrogen oxides. The  $\text{NO}_2$  observations

are consistent with previous studies of  $\text{O}_3$  at Blodgett Forest, which indicate chemical fluxes of  $\text{O}_3$  due to reactions with  $\text{NO}$  emitted from soil microbial processes (Kurpius and Goldstein, 2003). The upward fluxes of  $\Sigma\text{PNs}$  and  $\text{HNO}_3$  are likely due to within-canopy production following reaction of  $\text{NO}_2$  with  $\text{OH}$  and  $\text{RC}(\text{O})\text{O}_2$  radicals produced during VOC oxidation.  $\text{OH}$  mixing ratios within the canopy at Blodgett Forest have been estimated as between  $0.8$ – $3 \times 10^7$  molecules  $\text{cm}^{-3}$  as a result of oxidation of VOCs by  $\text{O}_3$  (Goldstein et al., 2004). We speculate that these high  $\text{OH}$  mixing ratios are adequate to produce enough within-canopy  $\text{HNO}_3$  to affect the observed fluxes. Similarly the  $\text{OH}$  may affect  $\Sigma\text{ANs}$  and  $\Sigma\text{PNs}$  through various chemical cycles. This mechanism, and some possible alternatives that were incapable of describing the data, are presented in more detailed in Farmer and Cohen (2006)<sup>2</sup>. These data give a hint of the enormous potential for mechanistic studies of factors controlling N fluxes and processing of N by and within forest canopies that EC with TD-LIF provides.

## 9 Conclusions

We describe the application of TD-LIF for measuring eddy covariance fluxes of  $\text{NO}_2$ ,  $\Sigma\text{PNs}$ ,  $\Sigma\text{ANs}$ , and  $\text{HNO}_3$ . Spectral analysis of the data demonstrate that the TD-LIF measurements have the necessary time response and sensitivity to measure fluxes by eddy covariance, and that internal diagnostics and line locking procedures do not compromise the flux measurements. We evaluated sources of random error and possible biases in TD-LIF flux measurements; these are summarized in Table 2. Sensor separation, spectral attenuation in sample tubing, and instrument time response combine

<sup>2</sup>Farmer, D. K. and Cohen, R. C.: Forest nitrogen oxide emissions: Evidence for rapid chemistry within the canopy, submitted, 2006.

to produce a bias of less than 3.5% underestimation of day-time fluxes under typical atmospheric conditions. The laser chop cycle may contribute as much as a 1% random error. Both theoretical and experimental treatments of the contribution of instrument noise to flux error demonstrate that observed fluxes are not dominated by instrument noise. Zero air fluxes suggest that instrument noise typically contributes a random error of much less than 10% of the observed fluxes. Typical measurement errors in eddy covariance CO<sub>2</sub> fluxes range from <7% during the day to <12% at night (Baldocchi, 2003 and references therein). Thus the major source of error in individual half-hour eddy covariance measurements of both CO<sub>2</sub> and TD-LIF NO<sub>y</sub>i is likely the natural variability in turbulence, likely between 10 and 20% (Wesely and Hart, 1985). This short-term error in flux measurements is reduced by applying longer-term averages of daily, weekly, or monthly fluxes (Baldocchi, 2003; Goulden et al., 1996).

Initial observations at Blodgett Forest demonstrate that TD-LIF has the potential to shed light on the complexity of ecosystem-level exchange of the reactive nitrogen oxides. Winter fluxes at Blodgett Forest are dominated by deposition of HNO<sub>3</sub>, ΣANs and ΣPNs. Within-canopy chemistry and the more complex factors controlling summer fluxes will be the subject of further study.

*Acknowledgements.* This research was supported by the NSF Atmospheric Chemistry Program under grant ATM-0138669. We gratefully acknowledge D. Day, E. Conlisk and I. Faloon for their contributions in the early stages of this project. Special thanks to the staff at UC-BFRS, in particular S. and D. Rambeau, for exceptional logistical support.

Edited by: W. E. Asher

## References

- Aber, J., McDowell, W., Nadelhoffer, K., Magill, A., Berntson, G., Kamakea, M., McNulty, S., Currie, W., Rustad, L., and Fernandez, I.: Nitrogen saturation in temperate forest ecosystems: Hypotheses revisited, *Biosci.*, 48, 921–934, 1998.
- Allan, J. D., Alfara, M. R., Bower, K. N., Coe, H., Jayne, J. T., Worsnop, D. R., Aalto, P. P., Kulmala, M., Hyotylainen, T., Cavalli, F., and Laaksonen, A.: Size and composition measurements of background aerosol and new particle growth in a Finnish forest during QUEST 2 using an Aerodyne Aerosol Mass Spectrometer, *Atmo. Chem. Phys.*, 6, 315–327, 2006.
- Anderson, D. E., Verma, S. B., Clement, R. J., Baldocchi, D. D., and Matt, D. R.: Turbulence spectra of CO<sub>2</sub>, water vapor, temperature, and velocity over a deciduous forest, *Agr. Forest Meteorol.*, 38, 81–99, 1986.
- Baldocchi, D. D., Hicks, B. B., and Meyers, T. P.: Measuring biosphere-atmosphere exchanges of biologically related gases with micrometeorological methods, *Ecology*, 69, 1331–1340, 1988.
- Baldocchi, D. D.: Assessing the eddy covariance technique for evaluating carbon dioxide exchange rates of ecosystems: past, present and future, *Glob. Change Biol.*, 9, 479–492, 2003.
- Bertram, T. H. and Cohen, R. C.: A prototype instrument for the detection of semi-volatile organic and inorganic nitrate aerosol, *Eos Trans. AGU*, 84, 2003.
- Bertram, T. H., Heckel, A., Richter, A., Burrows, J. P., and Cohen, R. C.: Satellite measurements of daily variations in soil NO<sub>x</sub> emissions, *Geophys. Res. Lett.*, 32, L24812, doi:10.1029/2005GL024640, 2005.
- Blanken, P. D., Black, T. A., Neumann, H. H., Den Hartog, G., Yang, P. C., Nestic, Z., Staebler, R., Chen, W., and Novak, M. D.: Turbulent flux measurements above and below the overstory of a boreal aspen forest, *Bound-Lay Meteorol.*, 89, 109–140, 1998.
- Bobbink, R., Heil, G. W., and Raessen, M. B. A. G.: Atmospheric Deposition and Canopy Exchange Processes in Heathland Ecosystems, *Environmental Pollution*, 75, 29–37, 1992.
- Bragazza, L. and Limpens, J.: Dissolved organic nitrogen dominates in European bogs under increasing atmospheric N deposition, *Global Biogeochem. Cycles*, 18, GB4018, doi:10.1029/2004GB002267, 2004.
- Brost, R., Delany, A., and Huebert, B.: Numerical modeling of concentrations and fluxes of HNO<sub>3</sub>, NH<sub>3</sub> and NH<sub>4</sub>NO<sub>3</sub> near the surface, *J. Geophys. Res.*, 93, 7137–7152, 1988.
- Bytnerowicz, A. and Riechers, G.: Nitrogenous Air-Pollutants in a Mixed-Conifer Stand of the Western Sierra-Nevada, California, *Atmos. Environ.*, 29, 1369–1377, 1995.
- Bytnerowicz, A. and Fenn, M. E.: Nitrogen deposition in California forests: A review, *Environmental Pollution*, 92, 127–146, 1996.
- Cleary, P. A., Murphy, J. G., Wooldridge, P. J., Day, D. A., Millet, D. B., McKay, M., Goldstein, A. H., and Cohen, R. C.: Observations of total alkyl nitrates within the Sacramento Urban Plume, *Atmos. Chem. Phys. Discuss.*, 5, 2005.
- Dabberdt, W. F., Lenschow, D. H., Horst, T. W., Zimmerman, P. R., Oncley, S. P., and Delany, A. C.: Atmosphere-surface exchange measurements, *Sci.*, 260, 1472–1481, 1993.
- Davidson, E. A. and Kinglerlee, W.: A global inventory of nitric oxide emissions from soils, *Nutrient Cycling in Agroecosystems*, 49, 37–50, 1997.
- Day, D. A., Wooldridge, P. J., Dillon, M. B., Thornton, J. A., and Cohen, R. C.: A thermal dissociation laser-induced fluorescence instrument for in situ detection of NO<sub>2</sub>, peroxy nitrates, alkyl nitrates, and HNO<sub>3</sub>, *J. Geophys. Res.*, 107, 4046, doi:10.1029/2001JD000779, 2002.
- Day, D. A., Dillon, M. B., Wooldridge, P. J., Thornton, J. A., Rosen, R. S., Wood, E. C., and Cohen, R. C.: On alkyl nitrates, O<sub>3</sub>, and the “missing NO<sub>y</sub>”, *J. Geophys. Res.*, 108, 4501, doi:10.1029/2003JD003685, 2003.
- Delany, A. C., Fitzjarrald, D. R., Lenschow, D. H., Pearson Jr., R., Wendel, G. J., and Woodruff, B.: Direct measurements of nitrogen oxides and ozone fluxes over grassland, *J. Atmos. Chem.*, 4, 429–444, 1986.
- Dillon, M. B., Lamanna, M. S., Schade, G. W., Goldstein, A. H., and Cohen, R. C.: Chemical evolution of the Sacramento urban plume: Transport and oxidation, *J. Geophys. Res.*, 107, 4045, doi:10.1029/2001JD000969, 2002.
- Domine, F. and Shepson, P. B.: Air-snow interactions and atmospheric chemistry, *Sci.*, 297, 1506–1510, 2002.
- Doskey, P. V., Kotamarthi, V. R., Fukui, Y., Cook, D. R., Breiteil

- III, F. W., and Wesely, M. L.: Air-surface exchange of peroxyacetyl nitrate at a grassland site, *J. Geophys. Res.*, 109, D10310, doi:10.1029/2004JD004533, 2004.
- Fenn, M. E., Poth, M. A., Aber, J. D., Baron, J. S., Bormann, B. T., Johnson, D. W., Lemly, A. D., McNulty, S. G., Ryan, D. F., and Stottlemeyer, R.: Nitrogen excess in North American ecosystems: Predisposing factors, ecosystem responses, and management strategies, *Ecological Applications*, 8, 706–733, 1998.
- Foken, T. and Wichura, B.: Tools for quality assessment of surface-based flux measurements, *Agricultural and Forest Meteorology*, 78, 83–105, 1996.
- Gasche, R. and Papen, H.: Spatial variability of NO and NO<sub>2</sub> flux rates from soil of spruce and beech forest ecosystems, *Plant and Soil*, 240, 67–76, 2002.
- Goldstein, A. H., Hultman, N. E., Fracheboud, J. M., Bauer, M. R., Panek, J. A., Xu, M., Wi, Y., Guenther, A. B., and Baugh, W.: Effects of climate variability on the carbon dioxide, water and sensible heat fluxes above a ponderosa pine plantation in the Sierra Nevada (CA), *Agricultural and Forest Meteorology*, 101, 113–129, 2000.
- Goldstein, A. H., McKay, M., Kurpius, M. R., Schade, G. W., Lee, A., Holzinger, R., and Rasmussen, R. A.: Forest thinning experiment confirms ozone deposition to forest canopy is dominated by reaction with biogenic VOCs, *Geophys. Res. Lett.*, 31, L22106, doi:10.1029/2004GL021259, 2004.
- Goulden, M. L., Munger, J. W., Fan, S. M., Daube, B. C., and Wofsy, S. C.: Measurements of carbon sequestration by long-term eddy covariance: Methods and a critical evaluation of accuracy, *Glob. Change Biol.*, 2, 169–182, 1996.
- Hanson, P. J. and Lindberg, S. E.: Dry deposition of reactive nitrogen compounds: A review of leaf, canopy and non-foliar measurements, *Atmos. Environ.*, 25A, 1615–1634, 1991.
- Hicks, B. B., Baldocchi, D. D., Meyers, T. P., Hosker, R. P., and Matt, D. R.: A Preliminary Multiple Resistance Routine for Deriving Dry Deposition Velocities from Measured Quantities, *Water Air Soil Poll.*, 36, 311–330, 1987.
- Hill, A. C.: Vegetation – Sink for Atmospheric Pollutants, *Japca J Air Waste Ma*, 21(6), 341–6, 1971.
- Holland, E. A., Braswell, B. H., Sulzman, J., and Lamarque, J.-F.: Nitrogen deposition onto the United States and Western Europe: Synthesis of observations and models, *Ecol. Appl.*, 15, 38–57, 2005.
- Horii, C. V.: Tropospheric reactive nitrogen speciation, deposition, and chemistry at Harvard Forest, PhD thesis, Harvard University, 2002.
- Horii, C. V., Munger, J. W., Wofsy, S. C., Zahniser, M., Nelson, D., and McManus, J. B.: Fluxes of nitrogen oxides over a temperate deciduous forest, *J. Geophys. Res.*, 109, D08305, doi:10.1029/2003JD004326, 2004.
- Horst, T. W.: A simple formula for attenuation of eddy fluxes measured with first-order-response scalar sensors, *Bound-Lay Meteorol.*, 82, 219–233, 1997.
- Huebert, B. J., Luke, W. T., Delany, A. C., and Brost, R. A.: Measurements of concentrations and dry surface fluxes of atmospheric nitrates in the presence of ammonia, *J. Geophys. Res.*, 93, 7127–7136, 1988.
- Jaegle, L., Martin, R. V., Chance, K., Steinberger, L., Kurosu, T. P., Jacob, D. J., Modi, A. I., Yoboue, V., Sigha-Nkamdjou, L., and Galy-Lacaux, C.: Satellite mapping of rain-induced nitric oxide emissions from soils, *J. Geophys. Res.*, 109, D21310, doi:10.1029/2004JD004787, 2004.
- Janson, R. and Granat, L.: A foliar rinse study of the dry deposition of nitric acid to a coniferous forest, *Agricultural and Forest Meteorology*, 98–99, 683–696, 1999.
- Kaimal, J. C., Wyngaard, J. C., Izumi, Y., and Cote, O. R.: Spectral characteristics of surface-layer turbulence, *Quarterly Journal of the Royal Meteorological Society*, 98, 563–589, 1972.
- Kurpius, M. R. and Goldstein, A. H.: Gas-phase chemistry dominates O<sub>3</sub> loss to a forest, implying a source of aerosols and hydroxyl radicals to the atmosphere, *Geophys. Res. Lett.*, 30, 1371–1375, doi:10.1029/2002GL016785, 2003.
- Lefter, B. L., Talbot, R. W., and Munger, J. W.: Nitric acid and ammonia at a rural northeastern U.S. site, *J. Geophys. Res.*, 104, 1645–1662, 1999.
- Lenschow, D. H. and Kristensen, L.: Uncorrelated noise in turbulence measurements, *J. Atmospheric and Oceanic Technology*, 2, 68–81, 1985.
- Lenschow, D. H. and Raupach, M. R.: The attenuation of fluctuations in scalar concentrations through sampling tubes, *J. Geophys. Res.*, 96, 15 259–15 268, 1991.
- Ludwig, J., Meixner, F. X., Vogel, B., and Forstner, J.: Soil-air exchange of nitric oxide: An overview of processes, environmental factors, and modeling studies, *Biogeochemistry*, 52, 225–257, 2001.
- Massman, W. J.: The attenuation of concentration fluctuations in turbulent flow through a tube, *J. Geophys. Res.*, 96, 15 269–15 274, 1991.
- Massman, W. J. and Lee, X.: Eddy covariance flux corrections and uncertainties in long-term studies of carbon and energy exchanges, *Agricultural and Forest Meteorology*, 113, 121–144, 2002.
- McMillen, R. T.: An eddy correlation technique with extended applicability to non-simple terrain, *Bound-Lay Meteorol.*, 43, 231–245, 1988.
- Moore, C. J.: Frequency response corrections for eddy correlation systems, *Bound-Lay Meteorol.*, 37, 17–36, 1986.
- Mosier, A., Wassman, R., Verchot, L., King, J. and Palm, C.: Methane and nitrogen oxide fluxes in tropical agricultural soils: Sources, sinks and mechanisms, *Environment, Development and Sustainability*, 6, 11–49, 2004.
- Munger, J. W., Wofsy, S. C., Bakwin, P. S., Fan, S.-M., Goulden, M. L., Daube, B. C., Goldstein, A. H., Moore, K. E., and Fitzjarrald, D. R.: Atmospheric deposition of reactive nitrogen oxides and ozone in a temperate deciduous forest and a subarctic woodland. 1. Measurements and mechanisms, *J. Geophys. Res.*, 101, 12 639–12 657, 1996.
- Munger, J. W., Fan, S.-M., Bakwin, P. S., Goulden, M. L., Goldstein, A. H., Colman, A. S. and Wofsy, S. C.: Regional budgets for nitrogen oxides from continental sources: Variations of rates for oxidation and deposition with season and distance from source regions, *J. Geophys. Res.*, 103, 8355–8368, 1998.
- Murphy, J. G., Day, D. A., Cleary, P. A., Wooldridge, P. J., and Cohen, R. C.: Observations of the diurnal and seasonal trends in nitrogen oxides in the western Sierra Nevada, *Atmos. Chem. Phys. Discuss.*, 6, 4415–4464, 2006, <http://www.atmos-chem-phys-discuss.net/6/4415/2006/>.
- Neff, J. C., Holland, E. A., Dentener, F. J., McDowell, W. H., and Russell, K. M.: The origin, composition and rates of organic ni-

- trogen deposition: A missing piece of the nitrogen cycle?, *Biogeochemistry*, 57/58, 99–136, 2002.
- Neffel, A., Blatter, A., Hesterberg, R., and Staffelbach, T.: Measurements of concentration gradients of HNO<sub>2</sub> and HNO<sub>3</sub> over a semi-natural ecosystem, *Atmos. Environ.*, 30, 3017–3025, 1996.
- Nemitz, E., Sutton, M. A., Wyers, G. P. and Jongejan, P. A. C.: Gas-particle interactions above a Dutch heathland: 1. Surface exchange fluxes of NH<sub>3</sub>, SO<sub>2</sub>, HNO<sub>3</sub> and HCl, *Atmos. Chem. Phys.*, 4, 989–1005, 2004, <http://www.atmos-chem-phys.net/4/989/2004/>.
- Neuman, J. A., Huey, L. G., Ryerson, T. B., and Fahey, D. W.: Study of inlet materials for sampling atmospheric nitric acid, *Environ. Sci. Technol.*, 33, 1133–6, 1999.
- Ollinger, S. V., Aber, J. D., Reich, P. B., and Freuder, R. J.: Interactive effects of nitrogen deposition, tropospheric ozone, elevated CO<sub>2</sub> and land use history on the carbon dynamics of northern hardwood forests, *Glob. Change Biol.*, 8, 545–562, 2002.
- Perakis, S. S. and Hedin, L. O.: Nitrogen loss from unpolluted South American forests via dissolved organic compounds, *Nature*, 415, 416–419, 2002.
- Pryor, S. C., Barthelmie, R. J., Jensen, B., Jensen, N. O., and Sorensen, L. L.: HNO<sub>3</sub> fluxes to a deciduous forest derived using gradient and REA methods, *Atmos. Environ.*, 36, 5993–5999, 2002.
- Ritter, J. A., Lenschow, D. H., Barrick, J. D. W., Gregory, G. L., Sachse, G. W., Hill, G. F., and Woerner, M. A.: Airborne flux measurements and budget estimates of trace species over the Amazon Basin during the GTE/ALBE 2B expedition, *J. Geophys. Res.*, 95, 16 875–16 886, 1990.
- Rosen, R. S., Wood, E. C., Wooldridge, P. J., Thornton, J. A., Day, D. A., Kuster, W., Williams, E. J., Jobson, B. T., and Cohen, R. C.: Observations of total alkyl nitrates during Texas Air Quality Study 2000: Implications for O<sub>3</sub> and alkyl nitrate photochemistry, *J. Geophys. Res.*, 109, D07303, doi:10.1029/2003JD004227, 2004.
- Rummel, U., Ammann, C., Gut, A., Meixner, G. X., and Andreae, M. O.: Eddy covariance measurements of nitric oxide flux within an Amazonian rain forest, *J. Geophys. Res.*, 107, 8050, doi:10.1029/2001JD000520, 2002.
- Schlesinger, W. H. and Andrews, J. A.: Soil respiration and the global carbon cycle, *Biogeochemistry*, 48, 7–20, 2000.
- Schrimpf, W., Lienaerts, K., Muller, K. P., Rudolph, J., Neubert, R., Schubler, W., and Levin, I.: Dry deposition of peroxyacetyl nitrate (PAN): Determination of its deposition velocity at night from measurements of the atmospheric PAN and <sup>222</sup>Rn concentration gradient, *Geophys. Res. Lett.*, 23, 3599–3602, 1996.
- Shepard, J. P., Mitchell, M. J., Scott, T. J., Zhang, Y. M., and Raynal, D. J.: Measurements of Wet and Dry Deposition in a Northern Hardwood Forest, *Water Air Soil Poll.*, 48, 225–238, 1989.
- Shepson, P. B., Bottenheim, J. W., Hastie, D. R., and Venkatram, A.: Determination of the Relative Ozone and Pan Deposition Velocities at Night, *Geophys. Res. Lett.*, 19, 1121–1124, 1992.
- Sievering, H., Kelly, T., McConville, G., Seibold, C., and Turnipseed, A.: Nitric acid dry deposition to conifer forests: Niwot Ridge spruce-fir-pine study, *Atmos. Environ.*, 35, 3851–3869, 2001.
- Sparks, J. P., Monson, R. K., Sparks, K. L., and Lerday, M.: Leaf uptake of nitrogen dioxide (NO<sub>2</sub>) in a tropical wet forest: implications for tropospheric chemistry, *Oecologia*, 127, 214–221, 2001.
- Sparks, J. P., Roberts, M. J., and Monson, R. K.: The uptake of gaseous organic nitrogen by leaves: A significant global nitrogen transfer process, *Geophys. Res. Lett.*, 30, 2189–2292, 2003.
- Su, H. B., Schmid, H. P., Grimmond, C. S. B., Vogel, C. S., and Oliphant, A. J.: Spectral characteristics and correction of long-term eddy-covariance measurements over two mixed hardwood forests in non-flat terrain, *Bound.-Lay. Meteorol.*, 110, 213–253, 2004.
- Tarnay, L., Gertler, A. W., Blank, R. R., and Taylor Jr., G. E.: Preliminary measurements of summer nitric acid and ammonia concentrations in the Lake Tahoe Basin air-shed: implications for dry deposition of atmospheric nitrogen, *Environmental Pollution*, 113, 145–153, 2001.
- Teklemariam, T. A. and Sparks, J. P.: Gaseous fluxes of peroxyacetyl nitrate (PAN) into plant leaves, *Plant, Cell and Environment*, 27, 1149–1158, 2004.
- Thornton, J. A., Wooldridge, P. J., and Cohen, R. C.: Atmospheric NO<sub>2</sub>: In situ laser-induced fluorescence detection at parts per trillion mixing ratios, *Analytical Chemistry*, 72, 528–539, 2000.
- Thornton, J. A., Wooldridge, P. J., Cohen, R. C., Williams, E. J., Hereid, D. P., Fehsenfeld, F. C., Stutz, J., and Alicke, B.: Comparisons of in situ and long path measurements of NO<sub>2</sub> in urban plumes, *J. Geophys. Res.*, 108, 4496, doi:10.1029/2003JD003559, 2003.
- Turnipseed, A. A., Huey, L. G., Nemitz, E., Stickel, R., Higgs, J., Tanner, D. J., Slusher, D. L., Sparks, J. P., Flocke, F., and Guenther, A.: Eddy covariance fluxes of peroxyacetyl nitrates (PANs) and NO<sub>y</sub> to a coniferous forest, *J. Geophys. Res.-Atmos.*, 111, D09304, doi:09310.01029/02005JD006631, 2006.
- Van Oss, R., Duyzer, J. and Wyers, P.: The influence of gas-to-particle conversion on measurements of ammonia exchange over forest, *Atmos. Environ.*, 32, 465–471, 1998.
- Vila-Guerau de Arellano, J., Duynkerke, P. G., and Builtjes, P. J. H.: The divergence of the turbulent diffusion flux in the surface layer due to chemical reactions: the NO-O<sub>3</sub>-NO<sub>2</sub> system, *Tellus*, 45B, 23–33, 1993.
- Vitousek, P. M., Aber, J. D., Howarth, R. W., Likens, G. E., Matson, P. A., Schindler, D. W., Schlesinger, W. H., and Tilman, D. G.: Human alteration of the global nitrogen cycle: Sources and consequences, *Ecol. Appl.*, 7, 737–750, 1997.
- Webb, E. K., Pearman, G. I., and Leuning, R.: Correction of flux measurements for density effects due to heat and water vapour transfer, *Quarterly Journal of the Royal Meteorological Society*, 106, 85–100, 1980.
- Wesely, M. L., Eastman, J. A., Stedman, D. H., and Yalvac, E. D.: An eddy-correlation measurement of NO<sub>2</sub> flux to vegetation and comparison to O<sub>3</sub> flux, *Atmos. Environ.*, 16, 815–820, 1982.
- Wesely, M. L. and Hicks, B. B.: A review of the current status of knowledge on dry deposition, *Atmos. Environ.*, 34, 2261–2282, 2000.
- Wildt, J., Kley, D., Rockel, A., Rockel, P., and Segschneider, H. J.: Emission of NO from several higher plant species, *JGR*, 102, 5919–5927, 1997.
- Zhang, Q., Carroll, J. J., Dixon, A. J., and Anastasio, C.: Aircraft measurements of nitrogen and phosphorus in and around the Lake Tahoe Basin: Implications for possible sources of atmospheric pollutants to Lake Tahoe, *Environ. Sci. Technol.*, 36, 4981–9, 2002.